Future Energy Open Access Journal

ISSN 2832-0328

Journal homepage: https://fupubco.com/fuen



https://doi.org/10.55670/fpll.fuen.5.1.3

Article

Advanced passive heat transfer enhancement: numerical analysis of TiO₂-water nanofluid flow in tubes fitted with twisted tape and conical ring inserts

Itquan Hossen*, Prasanjit Das, Ashraful Zannat Akhi

Department of Mechanical Engineering, Chittagong University of Engineering and Technology, Chittagong-4349, Bangladesh

ARTICLE INFO

Article history: Received 10 September 2025 Received in revised form 25 October 2025 Accepted 09 November 2025

Keywords:

Twisted tape, TiO₂ nanofluid, Passive heat transfer enhancement, Friction factor, Nusselt number, Thermal performance factor

*Corresponding author Email address: itquan2013@gmail.com

DOI: 10.55670/fpll.fuen.5.1.3

ABSTRACT

The primary objective of this study is to investigate the heat transfer enhancement, friction factor, and thermal performance factor of a plain tube with single and double twisted tapes, combined with a semicircular cut with and without dimples, a perforated V-cut, and conical rings, using a TiO2-water nanofluid. Numerical simulations of tube flow and heat transfer were conducted. The nanofluid used in the simulations contains TiO2 nanoparticles at concentrations of 0.5% and 1.5% by volume. The nanofluid inlet temperature was set at 300 K, and boundary conditions were applied. The maximum heat transfer coefficient increases from plain tube to 88.2% and 71.42% at double twisted tape with perforated V-cut and semi-circular cut, respectively, with dimples in 0.5% and 1.5% TiO_2 concentrations. The maximum Nusselt number increased by 115.53% and 100.9% at double twisted tape with perforated v-cut and semi-circular cut with dimples compared to the plain tube in 0.5% and 1.5% TiO₂ concentrations, respectively. The simple tube with a perforated V-cut and a conical ring insert exhibits a 94.44% higher friction factor at a 1.5% TiO₂ concentration. The maximum thermal performance factor was found to be 2.04 for double twisted tapes at a 0.5% TiO₂ concentration. Additionally, this study presents contour plots of the velocity distribution, pressure distribution, temperature distribution, and turbulent kinetic energy.

1. Introduction

In thermal engineering, a device used for transferring thermal energy between fluids, whether that's between a solid surface and a liquid or between solid particles and a gas, is called a heat exchanger. Without the exchange of work or the application of external heat, these machines are used in heating, cooling, evaporation, condensation, and heat recovery [1]. Heat exchange performance improvement is of special significance, as improved heat transfer performance can translate into more compact systems, lower costs, and substantial energy savings [2,3]. Heat transfer improvement techniques are an effective way to realize these advantages. Active, passive, and compound are three significant classifications of heat transfer improvement methods. Active techniques involve the application of external sources of power, such as fluid injections, electric or magnetic fields, mechanical assistance, or surface vibration, to enhance heat transfer. Passive techniques utilize turbulators, roughened

surfaces, fine surfaces, coiled tape, dimples, and protrusions or nanofluids to enhance the thermal efficiency of the system without introducing any supplementary energy. To attain greater heat transfer rates than by each method alone, composite techniques combine active and passive solutions [4,5]. Passive solutions include twisted tape inserts, which have received substantial attention due to their ease of application, economy, and simplicity of installation [6]. Strips of metal are shaped into particular geometries and placed in fluid flow conduits to improve heat transfer. These inserts create interference with the thermal boundary layer, increasing convective heat transfer through swirl flow and turbulence. They also lead to a pressure drop, and hence a compromise between heat transfer improvement and frictional loss is unavoidable. To maximize thermal performance and minimize pressure loss, various twisted tape geometries have been investigated in recent studies [5].

The following is an overview of recent studies that investigate the thermal performance outcomes of various twisted tape designs. Wongcharee et al. [6] examined the thermal-hydraulic behavior of U-cut twisted tapes (U-TTs) under homogeneous heat flow conditions when inserted into a circular tube. Their work focused on twist ratios (y/w = 3.5and 4.0) and U-cut ratios (s/t = 0.5 to 3.0). The thermal performance factor (TPF) was found to be 1.28 when s/t = 0.5and y/w = 3.5, which was better than any other configuration. They observed that U-TTs with smaller U-cut ratios (s/t = 0.5to 2.0) exhibited a significantly higher Nusselt number compared to regular twisted tapes. For U-TTs, however, friction losses were regularly larger than for standard tapes [6]. Li et al. [7] quantitatively investigated employing hollow twisted tapes for heat transfer enhancement in laminar flow. Their studies showed that cross-hollow twisted tapes enhanced general heat transfer performance by 28.1% over ordinary tapes. Reducing the gap between the tube and the twisted tape also improved heat transfer, and four unilateral twisted tapes at Reynolds numbers above 600 produced ideal

Abed et al. [8] investigated forced convection heat transfer in a horizontal pipe with twisted-tape inserts under constant heat flow using a numerical method. Their working fluid was water; they investigated Reynolds number (4000 ≤ Re \leq 9000), twist ratio (4.0 \leq TR \leq 6.0), and heat flow (5000 \leq $q \le 10000 \text{ W/m}^2$). Their results showed that V-cut twisted tapes with a twist ratio of 4 offered the highest thermal performance factor (TPF = 4.45), surpassing simple twisted tapes (TPF = 4.19). Promvonge et al. [9] investigated heat transmission in a circular tube combined with conical-ring and twisted-tape inserts. Their tests, using air as the working fluid, revealed that the combined inserts raised the Nusselt number by up to 367%, thanks to the formation of reverse and swirl flows, which improved fluid mixing. Abbasian Arani and Amani studied the effect of tube diameter on the heat transmission ability of TiO₂-water nanofluids [10]. increasing turbulence, they demonstrated that tube size increases enhanced heat transfer and led to greater pressure drops. Kumar et al. [11] also demonstrated that double V-cut perforated twisted tapes significantly enhanced heat transfer, with the optimum result achieved at a twist ratio of 2. Nanofluid developments in recent years have also further extended the scope for enhancing heat transfer. Dagdevir and Ozceyhan [12] conducted a comparison study utilizing plain tube, perforated twisted tape, and dimpled twisted tape. Working with mixes of ethylene glycol and water, they found that the concentration of ethylene glycol in the mixtures degraded thermal-hydraulic performance.

For instance, Eiamsa-ard et al. [13] found that TiO₂-water nanofluids with a volume concentration of 0.21% improved heat transmission by 9.9–11.2%, while Weerapun [14] noted that nanofluids displayed a 6–11% greater convective heat transfer coefficient than baseline fluids. S. Eiamsa-ard [15] investigated the twin-twisted-tape heat exchanger tube TiO₂-water nanofluid heat transfer improvement. Heat transmission improved by 9.9-11.2% and thermal performance by 4.5% at 0.21% TiO₂ volume concentration. According to a review of previous studies, various approaches have been employed over the years to optimize heat exchange performance. Passive techniques

have previously been employed, utilizing a variety of inserts with different types of cuts, various types of fluids, including nanofluids, and surface modifications to reduce the thickness of the thermal boundary layer. As a result, the search for a suitable insert remains a significant challenge. This study focuses on the numerical investigation of heat transfer improvement with TiO₂-water nanofluid in a tube fitted with conical rings and modified twisted tapes. The combinations of twisted tapes used in this study are: single twisted tape with perforated v-cut (STPV), single twisted tape with semicircular cut (STSC), perforated v-cut twisted tape with conical rings (PVTC), double twisted tape with perforated v-cut and semicircular cut (DTT-1), double twisted tape with perforated v-cut and semicircular cut with dimples (DTT-2), and plain tube. As can be seen, these combinations of twisted tapes have not been used in previous studies. Therefore, the effect of these combinations on heat transfer enhancement remains unknown.

For nanofluids, TiO2 is utilized due to its superior performance compared to other nanomaterials. TiO₂ nanoparticles exhibit exceptional capabilities for enhancing thermal conductivity in nanofluids. TiO2-water nanofluids have been reported to exhibit a thermal conductivity enhancement of up to 37% at elevated temperatures. Thermal conductivity for TiO2 nanofluids ranges from 4-11.8 W/m·K, which is significantly higher than that of most base fluids, and hence is extremely suitable for use in heat transfer applications [16,17]. The thermal stability of TiO₂ is particularly noteworthy, as the material maintains its structure and function up to 1000-1200°C. This heat resistance is superior to that of several other nanomaterials, which can break down or become less effective at lower temperatures [18,19]. Moreover, TiO2 is non-toxic and safe for humans, giving it a significant advantage over other nanoparticles that may pose health or environmental risks. TiO₂ nanoparticles possess fairly good dispersibility in polar and nonpolar base fluids, especially with the use of sufficient dispersants [20]. In contrast to other commonly used nanoparticles, TiO2 exhibits similar or improved performance. This study investigates the effects of heat transfer enhancement of STSC, STPV, PVTC, DTT-1, and DTT-2, and assesses the Nusselt number, friction factor, and thermal performance factor (TPF) over a range of Reynolds numbers (5000-49800) and TiO₂ volume concentrations (0.5% and 1.5%). However, optimization of twisted tape design and volume concentration percentage of TiO2 in water are not done in this study. There is a scope for future study by optimizing these combinations of twisted tapes and nanofluids. The results of this study seek to shed light on heat exchanger designs for refrigeration, power plants, chemical processing, and electronic cooling systems.

2. Numerical modelling

2.1 Physical modeling

Three types of twisted tape were used to insert into a plain tube. The tapes were semicircular cut, perforated V-cut, and semicircular cut with dimples. The working fluid used was a TiO_2 -water nanofluid with varying concentrations. The fluid entered the tube at a specific inlet temperature and flowed through the 70 mm diameter section, where the testing would take place. The investigation was conducted within the range of Reynolds numbers of 5000 to 49800.

Detailed information on the geometry is given in Table 1. Figure 1 shows the physical model of the plain tube, STSC, STPV, PVTC, DTT-1, and DTT-2.

In this study, air will be used as the working fluid in the plain tube validation, and TiO_2 -water will be used as the working fluid with different concentrations. The thermophysical properties of TiO_2 are given in Table 2. The properties of air are listed in Table 3, which are used as the defaults in ANSYS.

Table 1. Dimensions of the physical model

| Plain tube length, L | 1500mm |
|--------------------------------------|--------|
| Tube inner diameter, d | 70mm |
| Twisted tape length, l | 1440mm |
| Tape width, w | 24mm |
| Tape thickness, t | 2mm |
| Pitch length of insert, y | 48mm |
| Twist ratio, TR= y/w | 2 |
| V cut width, W | 7mm |
| Depth of cut | 6mm |
| Perforated hole diameter | 6mm |
| Distance Between two holes | 12mm |
| Radius of Semicircular Cut | 6mm |
| Opposite Semicircular cut distance | 24mm |
| Diameter of dimple | 2 mm |
| Conical ring length, Y | 60mm |
| Ring inlet diameter, D_1 | 15mm |
| Ring outlet diameter, D ₂ | 25mm |
| Pitch length of ring, P | 240mm |
| Pitch ratio, PR=P/D ₁ | 4 |

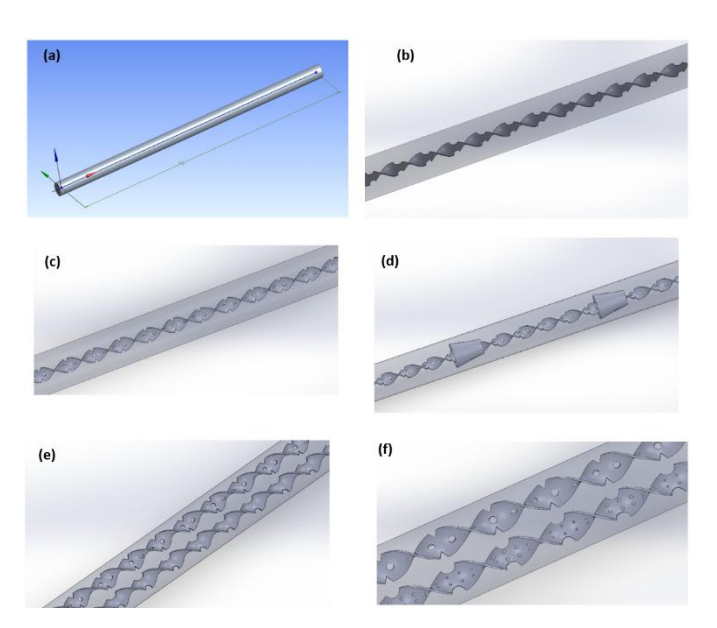


Figure 1. (a) 3D view of Plain Tube, (b) STSC, (c) STPV, (d) PVTC, (e) DTT-1, (f) DTT-2

2.2 Mesh generation

The term "mesh" refers to the abstract mathematical space utilized to generate polygons, tetrahedra, or hexahedra and other geometrical structures. Different mesh types are chosen based on geometric complexity, desired accuracy, and computational resources. Inadequate grid development, on the other hand, might reveal discrepancies from the intended mathematical design [22]. In this study, tetrahedron meshes were applied to the fluid domain for all of the geometries. The mesh size was 25 mm. A refined mesh was utilized along the tube wall to ensure the effect of the viscous sublayer. The first layer thickness inflation option was used to ensure that the y+ value remained below 1. Edge sizing with a particular number of divisions was applied to maintain meshing quality. Meshing criteria, such as orthogonal quality, skewness, and element quality, will be evaluated to determine mesh quality. Table 4 shows the meshing elements and summary. Figure 2 illustrates the meshing for the pipe wall, insert, and rings, which include holes and dimples.

Table 2. Properties of TiO₂ [21]

| Volume Concentration, φ (%) | Density, ρ (kg/m³) | Specific Heat, C _p (J/kg.K) | Thermal Conductivity, k (W/m k) | Viscosity, µ (kg/m.s) |
|-----------------------------------|--------------------------|--|---------------------------------------|-----------------------------|
| 0 | 1055.39 | 3502.0 | 0.413 | 0.00240 |
| 0.5 | 1071.26 | 3446.5 | 0.418 | 0.00251 |
| 1 | 1087.14 | 3392.7 | 0.418 | 0.00265 |
| 1.5 | 1103.01 | 3392.7 | 0.441 | 0.00279 |

Table 3. Properties of air

| Dynamic viscosity, μ | 1.7894×10 ⁻⁵ kg/m-s |
|-------------------------|--------------------------------|
| Specific heat, Cp | 1006.43 J/kg-k |
| Prandtl number, Pr | 0.744 |
| Air density, ρ | 1.225 kg/m ³ |
| Thermal conductivity, k | 0.242 W/m k |

Table 4. Meshing details

| Orthogonal quality | 0.99 | Transition ratio | 0.272 |
|-----------------------|---------------------|------------------|----------------------|
| Element size | 20 mm | Maximum layer | 10 |
| Edge sizing | Number of divisions | Inflation option | Smooth transition |
| Number of elements | 12000-19000 | node | 32096 |

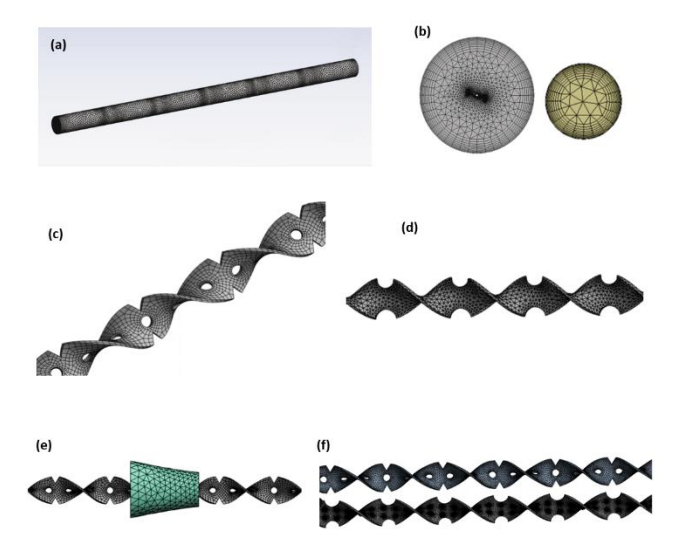


Figure 2. (a) Meshing profile for solid tube, (b) Inflation layer for tube wall, (c) Meshing profile for perforated v-cut twisted tape, (d) Meshing profile for semicircular cut twisted tape, (e) Meshing profile for perforated V-cut twisted tape with conical ring, (f) Meshing profile for double twisted tape with perforated v-cut and semi-circular cut with dimples

2.3 Governing equations

Mathematical modeling will be applied to anticipate flow and heat transfer characteristics. The finite difference method was used to evaluate the partial governing equations for boundary layers and swirling flows. Three governing equations characterize the properties of a fluid. The governing equations are solved by ANSYS Fluent, assuming the fluid is steady. The governing equations are used from Xie et al. [23]. The governing equations are given below.

$$\frac{\partial}{\partial x_i}(\rho u_i) = 0 \tag{1}$$

where ρ is fluid density, u_i is the ith-direction of flow velocity. Momentum equation:

$$\frac{\partial}{\partial x_j} \left(\rho u_i u_j \right) = -\frac{\partial \rho}{\partial x_i} + \frac{\partial}{\partial x_j} \left(\mu + \mu_t \right) \left(\frac{\partial u_i}{\partial x_j} + \frac{\partial u_j}{\partial x_i} \right) \tag{2}$$

where, u_i is the ith-direction of flow velocity, u_j is the jth-direction of flow velocity, μ is dynamic viscosity, μ_t is the eddy viscosity.

Energy equation:

$$\frac{\partial}{\partial x_i}(u_i T) = \frac{\partial}{\partial x_i} \left[\left(\frac{\mu}{Pr} + \frac{\mu_t}{Pr_t} \right) \frac{\partial T}{\partial x_i} \right] \tag{3}$$

where u_i is the ith-direction of flow velocity, T is temperature, μ is dynamic viscosity, μ_t is the eddy viscosity, Pr is the Prandtl number, and Pr_t is the Prandtl number of the turbulent flow.

Turbulent kinetic (Γ) energy equation:

$$\frac{\partial}{\partial x_i} (\rho k u_j) = \frac{\partial}{\partial x_i} \left[\left(\mu + \frac{\mu_t}{\sigma_k} \right) \frac{\partial k}{\partial x_i} \right] + \Gamma - \rho \epsilon \tag{4}$$

where ρ is fluid density, u_j is the jth-direction of flow velocity, μ is dynamic viscosity, μ_t is the eddy viscosity, Γ is the turbulent kinetic energy production rate, and ϵ is the dissipation rate of turbulent kinetic energy.

Specific dissipative rate (ε) equation:

$$\frac{\partial}{\partial x_{j}} \left(\rho \varepsilon u_{j} \right) = \frac{\partial}{\partial x_{j}} \left[\left(\mu + \frac{\mu_{t}}{\sigma_{\varepsilon}} \right) \frac{\partial \varepsilon}{\partial x_{j}} \right] + C_{1} \Gamma \varepsilon - C_{2} \frac{\varepsilon^{2}}{k + \sqrt{\nu} \varepsilon}$$
 (5)

where, $\sigma_k=1$ and $\sigma_\epsilon=1.3$, $C_1=m[0.43\,\frac{\mu_t}{\mu_t+5}]$ and $C_2=1$ and υ is the kinematic viscosity.

2.4 Simulation Setup

In this investigation, the energy equation was used in the ANSYS setup. When Nakhchi et al. [24] evaluated various turbulence models, including the standard k-model, the Renormalized Group (RNG) k-model, and the Shear Stress Transport (SST) k-model, they discovered that the (RNG) kmodel provides good accuracy. The RNG model of turbulence is derived from the instantaneous Navier-Stokes equations using a statistical method called "renormalization group" (RNG) methods. The RNG model improves accuracy for swirling flows by considering the effects of swirling on turbulence. The RNG viscous model with enhanced wall treatment was applied in this study. The use of y+ with enhanced wall treatment gives scalable benefits over standard wall functions. For solver parameters in the Fluent model setup, the pressure-based and steady-state models were used. Then, the RNG k- model for viscosity was chosen. The inlet temperature of air was taken to be 300K. The walls of STSC, STPV, PVTC, DTT-1, and DTT-2 were set to adiabatic walls. The boundary conditions are shown in Table 5.

Table 5. Boundary conditions

| Surface | Thermal | Momentum |
|--|-----------------------|-------------------|
| Inlet | 300k | Velocity inlet |
| Outlet | - | Pressure outlet |
| Tube wall | 7500 W/m ² | No-slip condition |
| Walls of all twisted tapes and conical rings | 0 W/m ² | - |

2.5 Numerical procedures

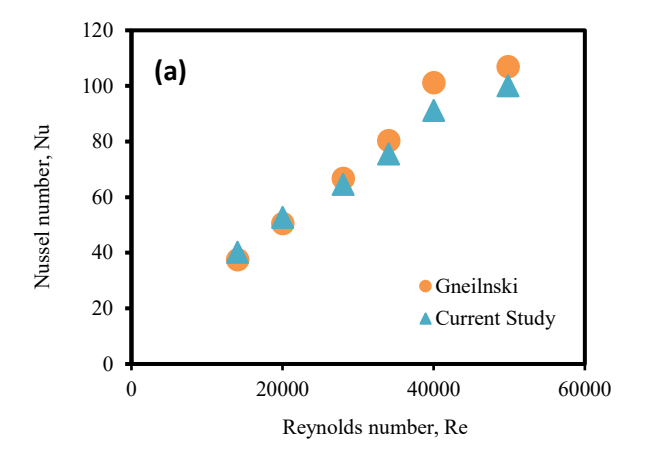
The pressure-based solver is used in this study to solve the steady-state problem. The governing equations are solved by the finite volume method. The SIMPLE (Semi-implicit Method for the Pressure-Linked Equations) algorithm was selected for the numerical study. Twisted tapes fitted with a plain tube were utilized with PRESTO (Pressure Staggering Option). The Quadratic Upstream Interpolation for Convective Kinematics (QUICK) approach employed momentum, energy, turbulent kinetic energy, and specific dissipation rate to obtain accuracy. When the residuals dropped below 10-3 the numerical solutions converged, except for the energy equation, which dropped below 10-6.

3. Results and discussion

3.1 Validation of simulations

In order to validate the simulation results for a plain tube to calculate heat transfer augmentation, the results are compared with the Gneilski correlation for Nusselt number comparison and the Petukhov correlation for friction factor [25]. A previous experimental work of Promvonge et al. [26] using a conical ring and a previous experimental investigation by Bhuiya et al. [27] was validated by simulation results.

The Gneilnski correlation was used to verify the plain tube for the Nusselt number. The Nusselt number deviation percentage ranges from 3.78% to 5.18% with an RMS error of 3.079%. The friction factor for the simple tube was confirmed using the Petukhov correlation [25]. The friction factor's deviation percentage varied from 6.3778% to 13.405%. with an RMS error of 2.837%. Figure 3 illustrates the validation results for the Nusselt number and friction factor.



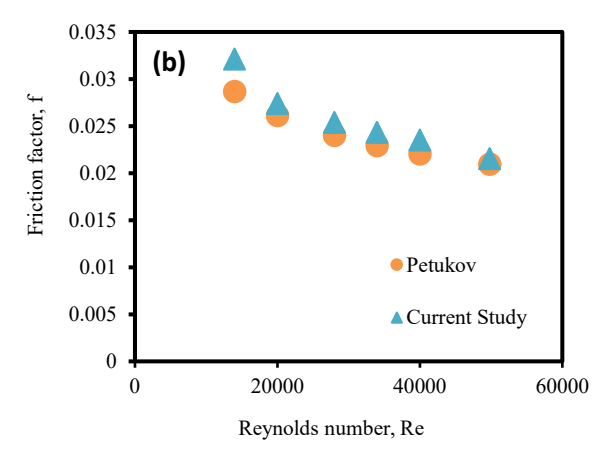


Figure 3. (a) Nusselt number validation for plain tube, (b) Friction factor validation

To ensure the simulation procedure validated a previous experimental work done by Promvonge et al. [28]. The working fluid for this experiment was air. The deviation percentage of the Nusselt number varied from 16.5% to 18.01%. The validation of the Nusselt number for a conical ring is shown in Figure 4.

3.2 Heat transfer enhancement characteristics

Heat transfer coefficient results from ANSYS Fluent were gathered. The connection between the Reynolds number and the heat transfer coefficient of double and single twisted tape inserts at various concentrations of TiO_2 is shown in Figure 5, which demonstrates that, in all cases, the heat transfer coefficient increased as the Reynolds number increased. The heat transfer rate increased because the twisted tapes created vortices and turbulence in the fluid flow, which ensured better fluid mixing and, consequently, increased the heat transfer rate [29]. Besides, twisted tapes create a larger effective surface area, which improves overall heat transfer performance. The Maximum Heat transfer coefficient is

increased from plain tube to 88.2% and 71.42% at PVTC and DTT-2 in 0.5% and 1.5% TiO_2 concentrations, respectively.

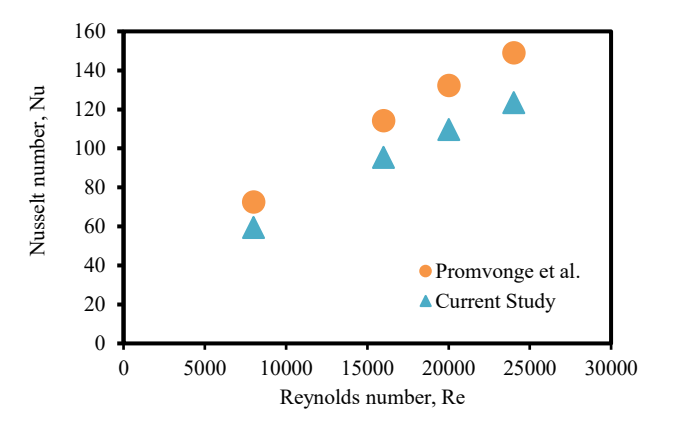
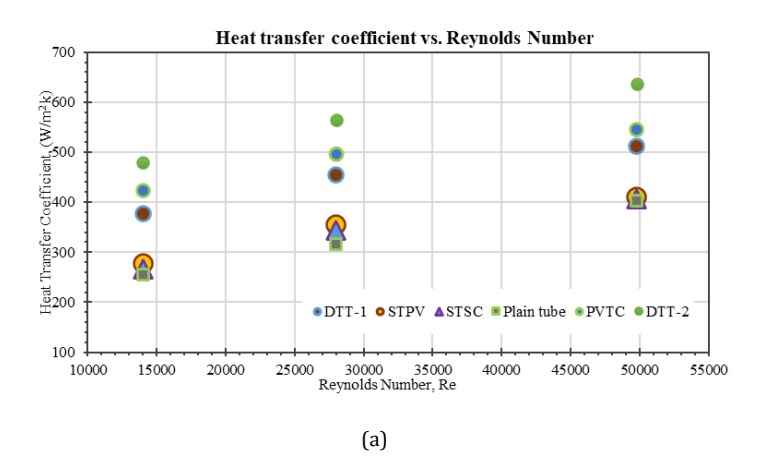


Figure 4. Nusselt number validation for a conical ring



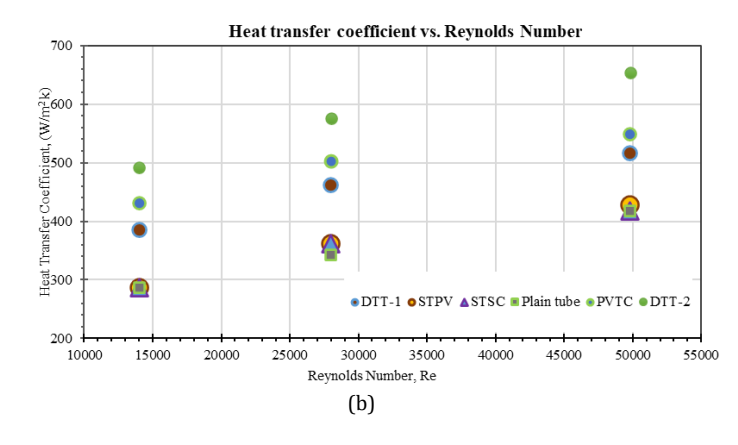
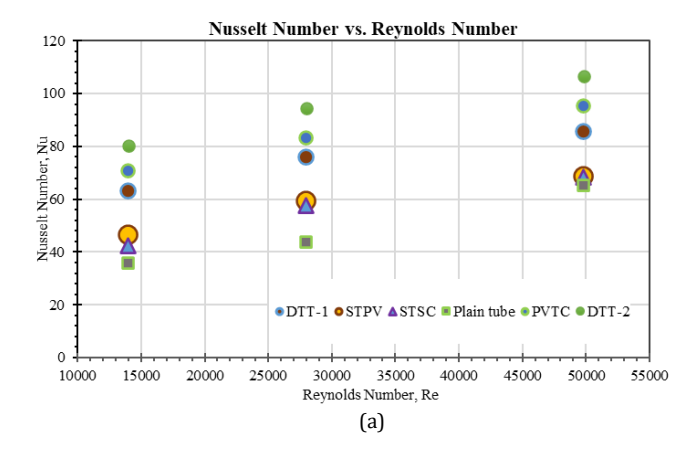


Figure 5. (a) Comparison of the Reynolds number and the heat transfer coefficient for 0.5% TiO₂, (b) Comparison of the Reynolds number and the heat transfer coefficient for 1.5% TiO₂

Figure 6 depicts the relationship between the Nusselt number and the Reynolds number. The maximum Nusselt number increased by 115.53% and 100.9% for double twisted tape with perforated V-cut and semi-circular cut with dimples, compared to the plain tube in 0.5% and 1.5% TiO_2 concentrations. Figure 6 illustrates that, in all instances, the Nusselt number increased as the Reynolds number increased.

Convective heat transfer was amplified as the intensity of turbulent flow increased with the Reynolds number. The twisted and double-twisted tapes swirl generators have a considerable impact on the heat transfer rate for all Reynolds numbers. This may produce secondary or swirl flow, which provides a longer channel for the fluid to flow through the tube. Intense fluid and pressure gradient mixing might also have been formed in the radial direction.



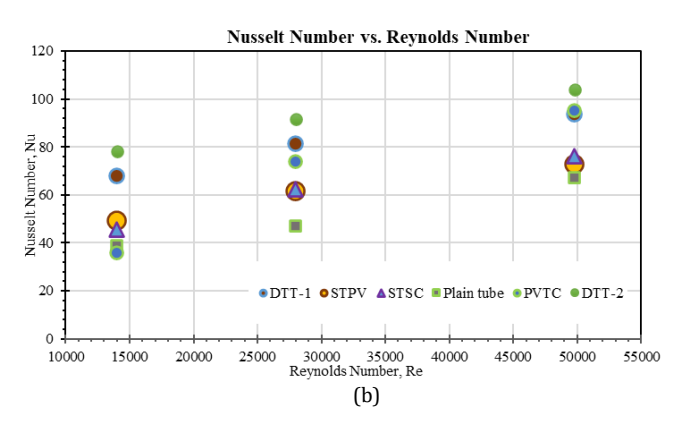
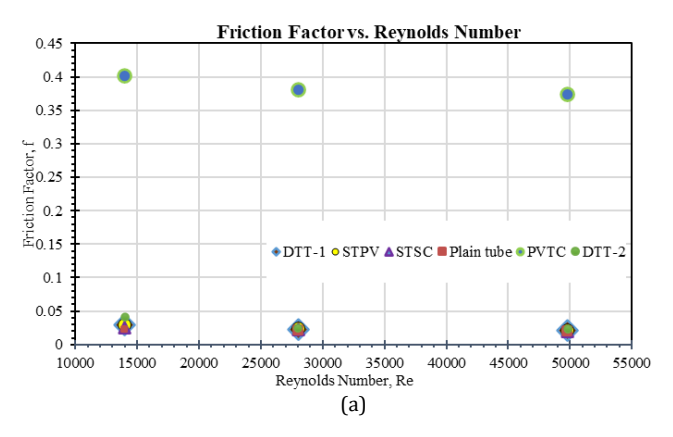


Figure 6. (a) Comparison of the Reynolds number and Nusselt number for 0.5% TiO2, (b) Comparison of the Reynolds number and Nusselt number for $1.5\%\ TiO_2$.

The friction factor was computed using the Darcy-Weisbach equation after collecting the pressure drop from the inlet to the outlet in the ANSYS Fluent results. Figure 7 shows the effects of double twisted tape inserts on friction factor characteristics. The friction factor of the tape-inserted tube steadily decreased as the Reynolds number rose. It is shown that the friction factor increased by a vast amount at lower Reynolds number values and by a relatively small amount at higher Reynolds number values. This might be explained by the fact that at lower Reynolds number values, which correspond to lower flow rates, air can travel over the tape and produce large frictional forces, as tiny vortices are present behind the tape. The friction coefficients of PVTC were 94.44% greater than those of the plain tube. When designing heat exchangers, the thermal performance factor (TPF) is very important. The TPF demonstrated the usefulness of using twisted tape in heat exchangers [29]. With an increase in Reynolds number, the performance characteristics for all twisted tapes tended to decline. This suggested that the energy-saving devices for usage at lower Reynolds numbers were the enhancement devices. Figure 8 shows the thermal performance factor using double and single twisted tapes for 10000 to 55000 Reynolds numbers. The maximum thermal performance factor was found at DTT-2. The maximum value of TPF is 2.04 and 1.88 at 0.5% and 1.5% TiO₂ concentrations, respectively.



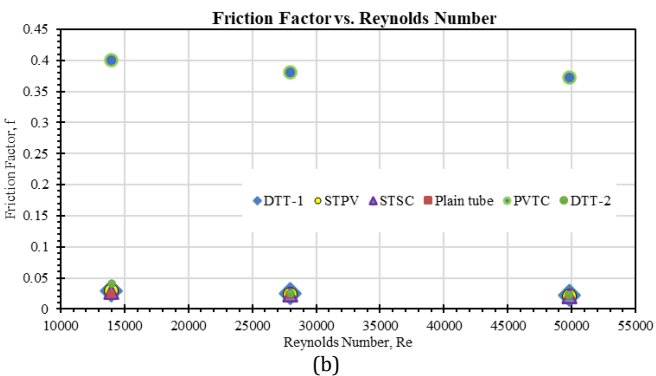


Figure 7. (a) Comparison of the Reynolds number and Friction factor for 0.5% TiO₂, (b) Comparison of the Reynolds number and Friction factor for 1.5% TiO₂

3.3 Contour plots

The velocity contour for the plain tube and STSC, PVTC, DTT-1, STPV, DTT-2 are shown in Figure 9. The fluid velocity reaches the free stream velocity at the center of the pipe and becomes zero adjacent to the pipe wall. Also, velocity increases at the tube's inlet region and decreases when the insert geometry restricts the passage.

The temperature distribution contour for the plain tube and STSC, STPV, PVTC, DTT-1, and DTT-2 are shown in Figure 9. For a plain tube, the temperature increases at the boundary layer adjacent to a solid surface. Figure 10 illustrates the temperature range from high to low at the boundary surface fluid. After using the insert on a plain tube, the heat was distributed everywhere, enhancing the heat transfer.

The pressure distribution contour for the plain tube and STSC, STPV, PVTC, DTT-1, and DTT-2 are shown in Figure 11. At the inlet section, pressure was higher, but a pressure drop occurred at the outlet section due to frictional forces. After using conical rings, fluid flow creates more disturbance because more pressure drop occurs in the outlet section.

Figure 12 shows the turbulent kinetic energy for various sections of plain tubes and tubes equipped with inserts. The contour figure shows that TKE is higher where the boundary is closest to the tube wall and also where the alternate axis dimpled twisted tape is located, indicating high shear stress.

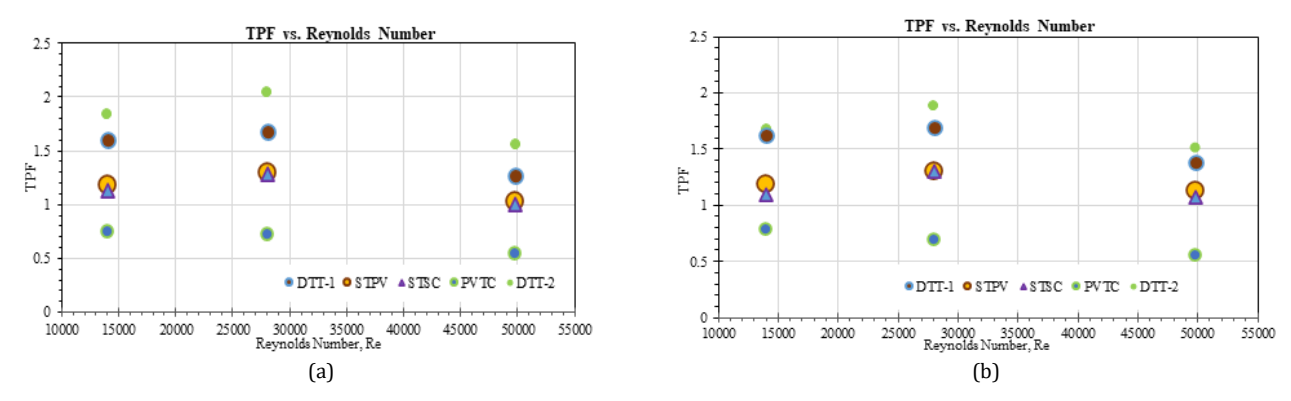


Figure 8. (a) Comparison of the Reynolds number and TPF for 0.5% TiO₂, (b) Comparison of the Reynolds number and TPF for 1.5% TiO₂

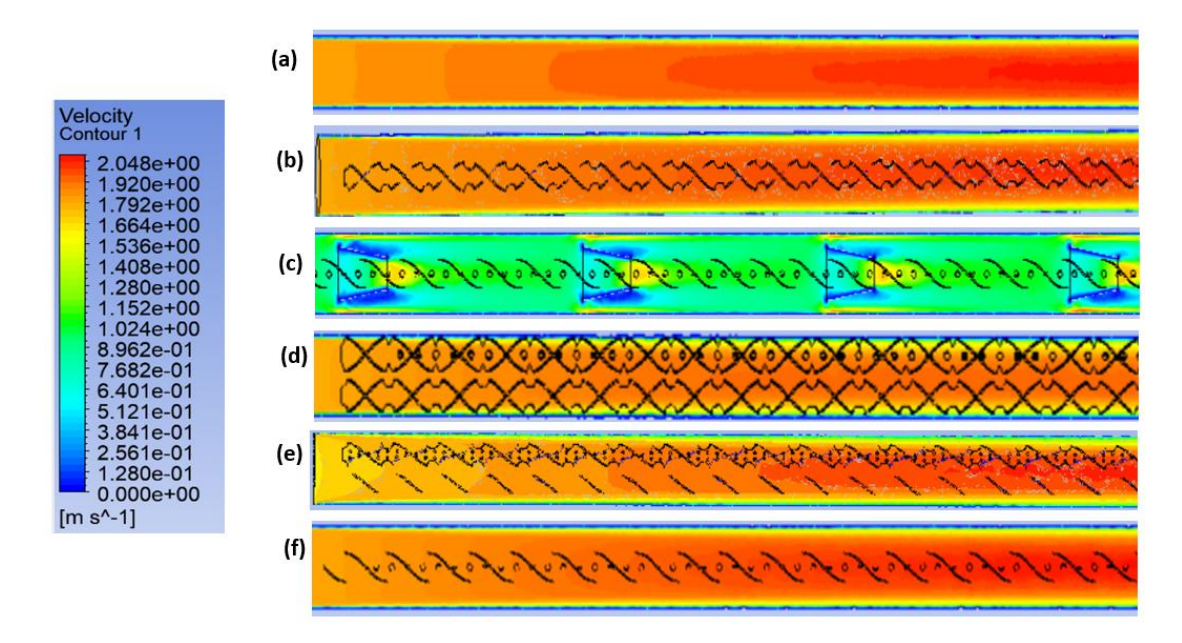
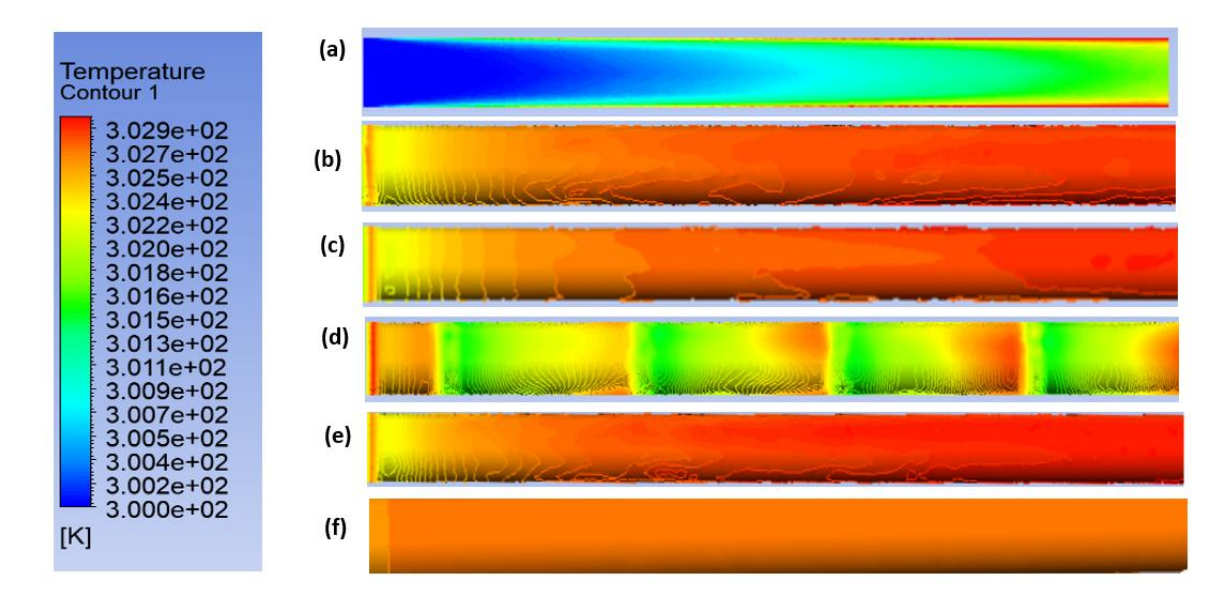


Figure 9. (a) Plain Tube, (b) STSC, (c) PVTC, (d) DTT-1, (e) DTT-2, (f) STPV



 $\textbf{Figure 10.} \ (a) \ Plain \ Tube, (b) \ STSC, (c) \ STPV, (d) \ PVTC, (e) \ DTT-1, (f) \ DTT-2$

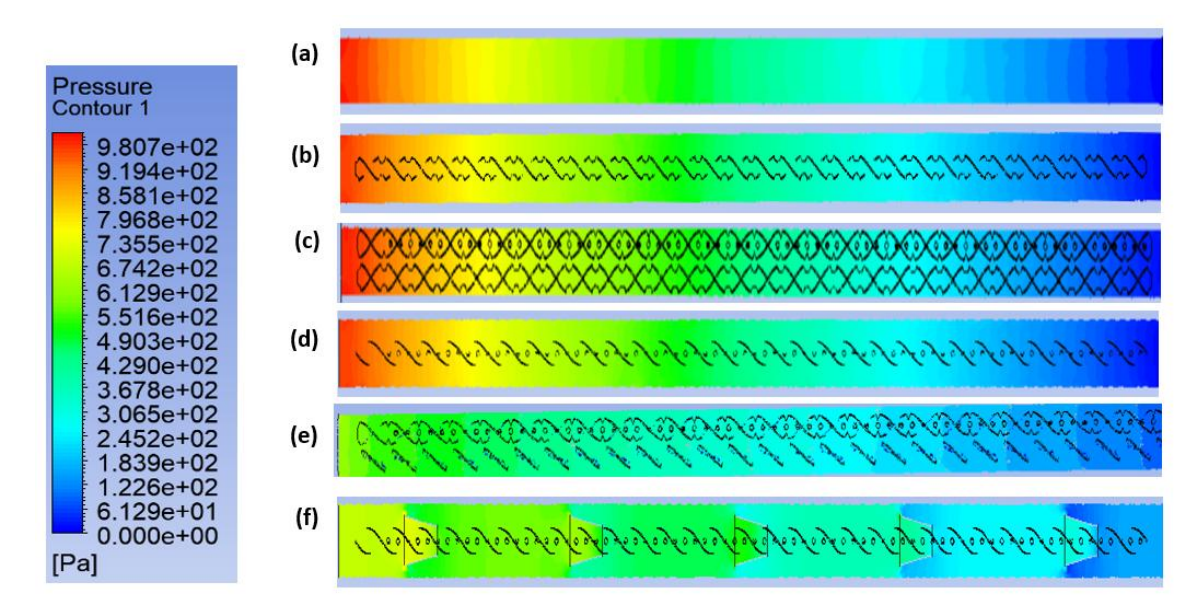


Figure 11. (a) Plain Tube, (b) STSC, (c) DTT-1, (d) STPV, (e) DTT-2, (f) PVTC

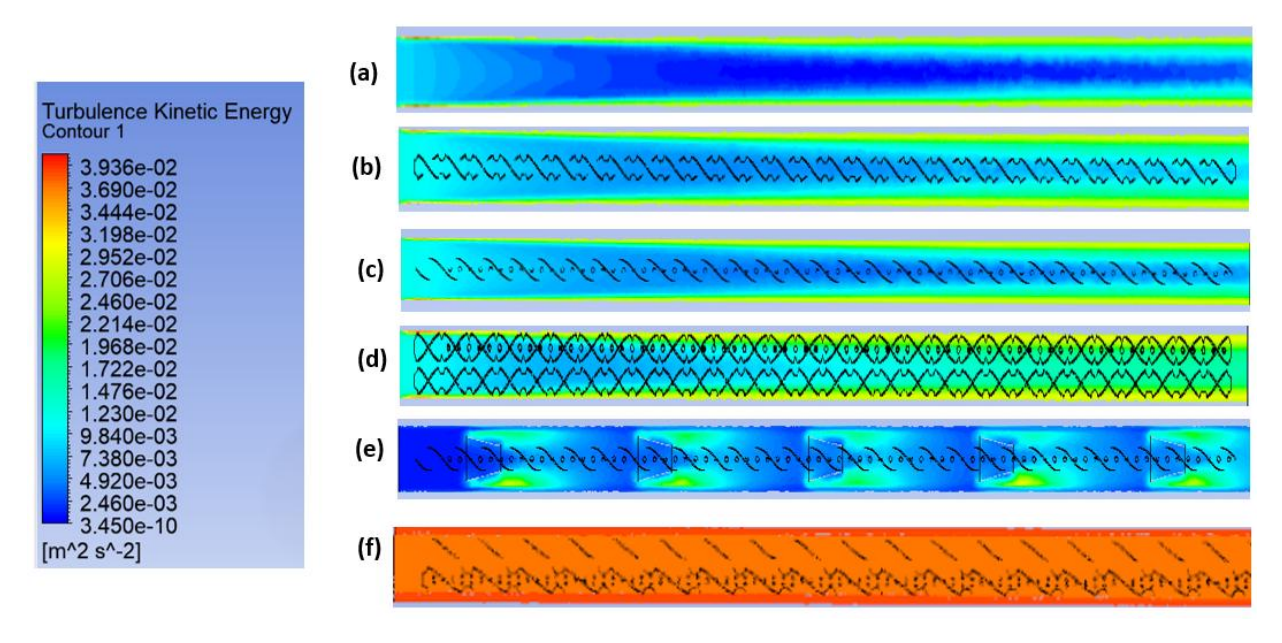


Figure 12. (a) Plain Tube, (b) STSC, (c) STPV, (d) DTT-1, (e) PVTC, (f) DTT-2

Velocity increases in the tube's inlet region and decreases when the insert geometry restricts the passage. For a plain tube, the temperature increases at the boundary layer adjacent to a solid surface. After using the insert on a plain tube, the heat was distributed everywhere, enhancing the heat transfer. At the inlet section, pressure was higher, but a pressure drop occurred at the outlet section due to frictional forces. After using double-twisted tape inserts, fluid flow creates more disturbance because a greater pressure drop occurs in the outlet section.

4. Conclusion

In the present research, the heat transfer and friction factor characteristics of turbulent flow for STSC, STPV, PVTC, DTT-1, and DTT-2 at varying TiO₂ concentrations were investigated numerically. When compared to the plain tube, the DTT-2 significantly boosted the heat transmission rate. The following are the primary findings of this numerical study:

 The double twisted tapes offered a higher heat transfer rate, friction factor, and thermal performance factor as compared to the plain tube. As the Reynolds number increased, so did the Nusselt number. The Maximum Heat transfer coefficient is increased from plain tube to 88.2% and 71.42% at DTT-2 in 0.5% and 1.5% TiO₂ concentrations, respectively. Also, the maximum Nusselt number rose by 115.53% and 100.9% at DTT-2 compared to the plain tube in 0.5% and 1.5% TiO₂ concentrations, respectively. The Nusselt number increased because the twisted tapes with insertion create vortices and turbulence in the fluid flow, which ensured better fluid mixing that increased the heat transfer rate. Besides, twisted tapes create a larger effective surface area, which improves overall heat transfer performance. There were four different cases. The Nusselt number was enhanced for double twisted tapes, perforated V-cut with and without conical ring, semicircular cut tape by 74.52%, 101.2%, 29.19%, 18.49% respectively for 1.5% of TiO₂ nanofluid and by 67.7231%, 97.32%, 26.2%, 18.23% respectively for 0.5% TiO₂ nanofluid.

- The friction factor decreased with the increase of the Reynolds number. The friction factor of a tube with a double twisted tape insert was higher than that of the plain tube. The maximum friction factor increased from that of a plain tube to 94.44% with a double twisted tape at a 1.5% TiO2 nano-fluid concentration. The friction factor was increased for double twisted tapes, perforated V-cut with and without conical ring, semicircular cut tape by 75.4%, 94.44%, 55.32%, 33.3078%, respectively for 1.5% of TiO2 nano fluid, and by 71.757%, 82.86%, 45.29%, 28.75% respectively for 0.5% TiO2 nano fluid.
- The thermal performance factor was also evaluated. The thermal performance factor decreased with increased Reynolds number. The maximum thermal performance factor was found to be 2.04 at a Reynolds number of 14000 for DTT-2 at a 0.5% concentration of TiO₂.

For further investigation, the cuts on the twisted tape can be modified. Also, the conical rings configuration can be changed as well. Since in this study conical rings with V-cut have been used, the hexagonal ring with V-cut or rectangular cut can be utilized to analyze the heat transfer enhancement. Besides, the pressure drop analysis can be done between the V-cut with conical ring configuration and the v/rectangular cut with hexagonal configuration.

Ethical issue

The authors are aware of and comply with best practices in publication ethics, specifically concerning authorship (avoidance of guest authorship), dual submission, manipulation of figures, competing interests, and compliance with policies on research ethics. The authors adhere to publication requirements that the submitted work is original and has not been published elsewhere in any language.

Data availability statement

The manuscript contains all the data. However, more data will be available upon request from the corresponding author.

Conflict of interest

The authors declare no potential conflict of interest.

References

- [1] Shah RK, Sekulib DR. Handbook of heat transfer 3 HEAT EXCHANGERS. 1998;3:17.1-17.169.
- [2] Webb RL, Kim NY. Enhanced heat transfer. Taylor & Samp 2005. ISBN: 1-59169-014-5
- [3] Khargotra R, Kumar R, Nadda R et al. A review of different twisted tape configurations used in heat exchanger and their impact on thermal performance of the system. Heliyon 2023;9:e16390.

- [4] Ajarostaghi SSM, Zaboli M, Javadi H et al. A Review of Recent Passive Heat Transfer Enhancement Methods. Energies (Basel) 2022;15, DOI: 10.3390/en15030986.
- [5] Tejas Sonawane M, Prafulla Patil M, Chavhan MA et al. a Review on Heat Transfer Enhancement By Passive Methodss. International Research Journal of Engineering and Technology 2016;3:1567-74.
- [6] Wongcharee K, Chuwattanakul V, Chamoli S et al. Investigation of turbulent thermal-hydraulic behaviors of a heat exchanger tube with U-cut twisted-tape. Case Studies in Thermal Engineering 2025;67:105838.
- [7] Li P, Liu Z, Liu W et al. Numerical study on heat transfer enhancement characteristics of tube inserted with centrally hollow narrow twisted tapes. Int J Heat Mass Transf 2015;88:481–91.
- [8] Abed AM, Sh Majdi H, Hussein Z et al. Numerical analysis of flow and heat transfer enhancement in a horizontal pipe with P-TT and V-Cut twisted tape. Case Studies in Thermal Engineering 2018;12:749–58.
- [9] Promvonge P, Eiamsa-ard S. Heat transfer behaviors in a tube with combined conical-ring and twisted-tape insert. International Communications in Heat and Mass Transfer 2007;34:849–59.
- [10] Arani AAA, Amani J. Experimental investigation of diameter effect on heat transfer performance and pressure drop of TiO2–water nanofluid. Exp Therm Fluid Sci 2013;44:520–33.
- [11] Kumar B, Patil AK, Jain S et al. Study of entropy generation in heat exchanger tube with multiple V cuts in perforated twisted tape insert. J Heat Transfer 2019;141:81801.
- [12] Dagdevir T, Uyanik M, Ozceyhan V. The experimental thermal and hydraulic performance analyses for the location of perforations and dimples on the twisted tapes in twisted tape inserted tube. International Journal of Thermal Sciences 2021;167:107033.
- [13] Eiamsa-ard S, Kiatkittipong K. Heat transfer enhancement by multiple twisted tape inserts and TiO2/water nanofluid. Appl Therm Eng 2014;70:896– 924.
- [14] Duangthongsuk W, Wongwises S. Heat transfer enhancement and pressure drop characteristics of TiO2–water nanofluid in a double-tube counter flow heat exchanger. Int J Heat Mass Transf 2009;52:2059–67.
- [15] Eiamsa-Ard S, Kiatkittipong K, Jedsadaratanachai W. Heat transfer enhancement of TiO2/water nanofluid in a heat exchanger tube equipped with overlapped dual twisted-tapes. Engineering Science and Technology, an International Journal 2015;18:336–50.
- [16] Alias H, Ani MFC. Thermal characteristic of nanofluids containing titanium dioxide nanoparticles in ethylene glycol. Chem Eng Trans 2017;56:1459–64.
- [17] Abdel-Samad SM, Fahmy AA, Massoud AA et al.
 Experimental Investigation of TiO2-water Nanofluids
 Thermal Conductivity Synthesized by Sol-gel
 Technique. Curr Nanosci 2017;13:586–94.

- [18] Ahmadlouydarab M, Javadi S, Darab FAA. Evaluation of Thermal Stability of TiO2 Applied on the Surface of a Ceramic Tile to Eliminate Methylene Blue Using Silica-based Doping Materials. Advanced Journal of Chemistry, Section A 2023;6:352–65.
- [19] Ferreira-Neto EP, Ullah S, Martinez VP et al. Thermally stable SiO2@TiO2core@shell nanoparticles for application in photocatalytic selfcleaning ceramic tiles. Mater Adv 2021;2:2085–96.
- [20] Yang L, Hu Y. Toward TiO(2) Nanofluids-Part 1: Preparation and Properties. Nanoscale Res Lett 2017;12:417.
- [21] Hamid KA, Azmi WH, Mamat R et al. Effect of temperature on heat transfer coefficient of titanium dioxide in ethylene glycol-based nanofluid. Journal of Mechanical Engineering and Sciences 2015;8:1367–75
- [22] Mesh Types In CFD: A Comprehensive Guide. https://www.ansys.com/products/fluids
- [23] V. Gnielinski. New equations for heat and mass transfer in turbulent pipe and channel flow. International Chemical Engineering 1976.
- [24] Nakhchi ME, Esfahani JA. Performance intensification of turbulent flow through heat exchanger tube using double V-cut twisted tape inserts. Chemical Engineering and Processing - Process Intensification 2019;141:107533.

- [25] Petukhov BS. Heat Transfer and Friction in Turbulent Pipe Flow with Variable Physical Properties. Adv Heat Transf 1970;6:503-64.
- [26] Moria H. Compound usage of twisted tape turbulator and air injection for heat transfer augmentation in a vertical straight tube with upward stream. Case Studies in Thermal Engineering 2021;25:100854.
- [27] Bhuiya MMK, Chowdhury MSU, Saha M et al. Heat transfer and friction factor characteristics in turbulent flow through a tube fitted with perforated twisted tape inserts. International Communications in Heat and Mass Transfer 2013;46:49–57.
- [28] Promvonge P, Eiamsa-ard S. Heat transfer behaviors in a tube with combined conical-ring and twisted-tape insert. International Communications in Heat and Mass Transfer 2007;34:849–59.
- [29] Kumar Sahu M, Kumar Singh S. Double-Sided Semi-Circular-Wing Tape Inserts to Enhance Thermal Performance of a Double-Pipe Heat Exchanger. International Journal of Recent Research in Civil and Mechanical Engineering (IJRRCME) 2020;7:1–8.



This article is an open-access article distributed under the terms and conditions of the Creative Commons Attribution (CC BY) license

(https://creativecommons.org/licenses/by/4.0/).